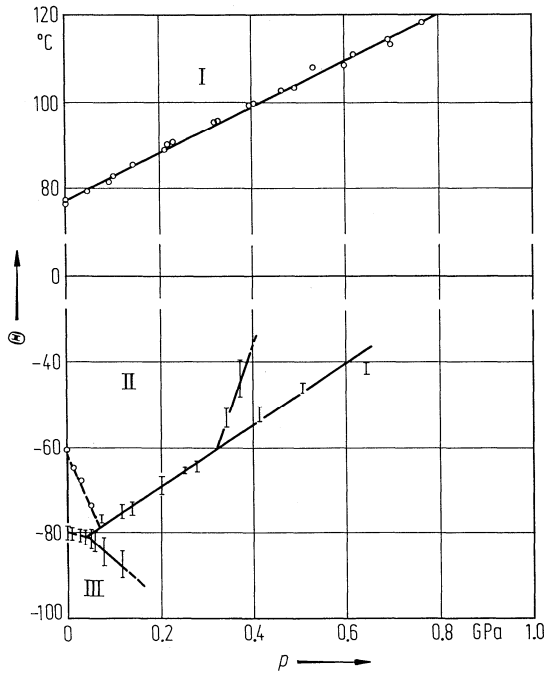

Fig. 39A-17-001. Rb_2ZnBr_4. Θ vs. p [85Ges]. Dashed line in phase II below 60 MPa corresponds to a slight step-like anomaly of κ_a.

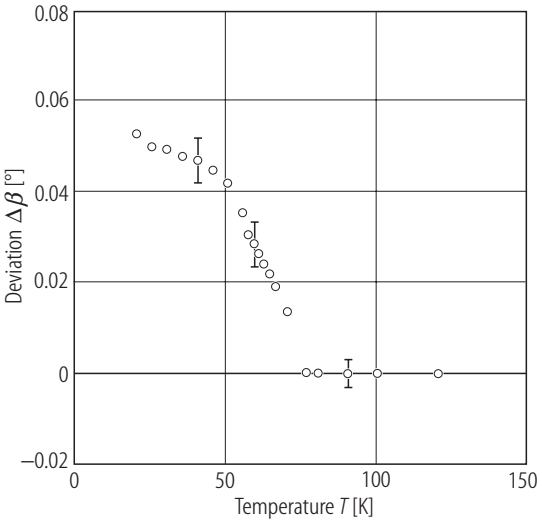

Fig. 39A-17-002. Rb_2ZnBr_4. $\Delta\beta$ vs. T [96Shi1]. $\Delta\beta$: deviation of axial angle β from 90°.

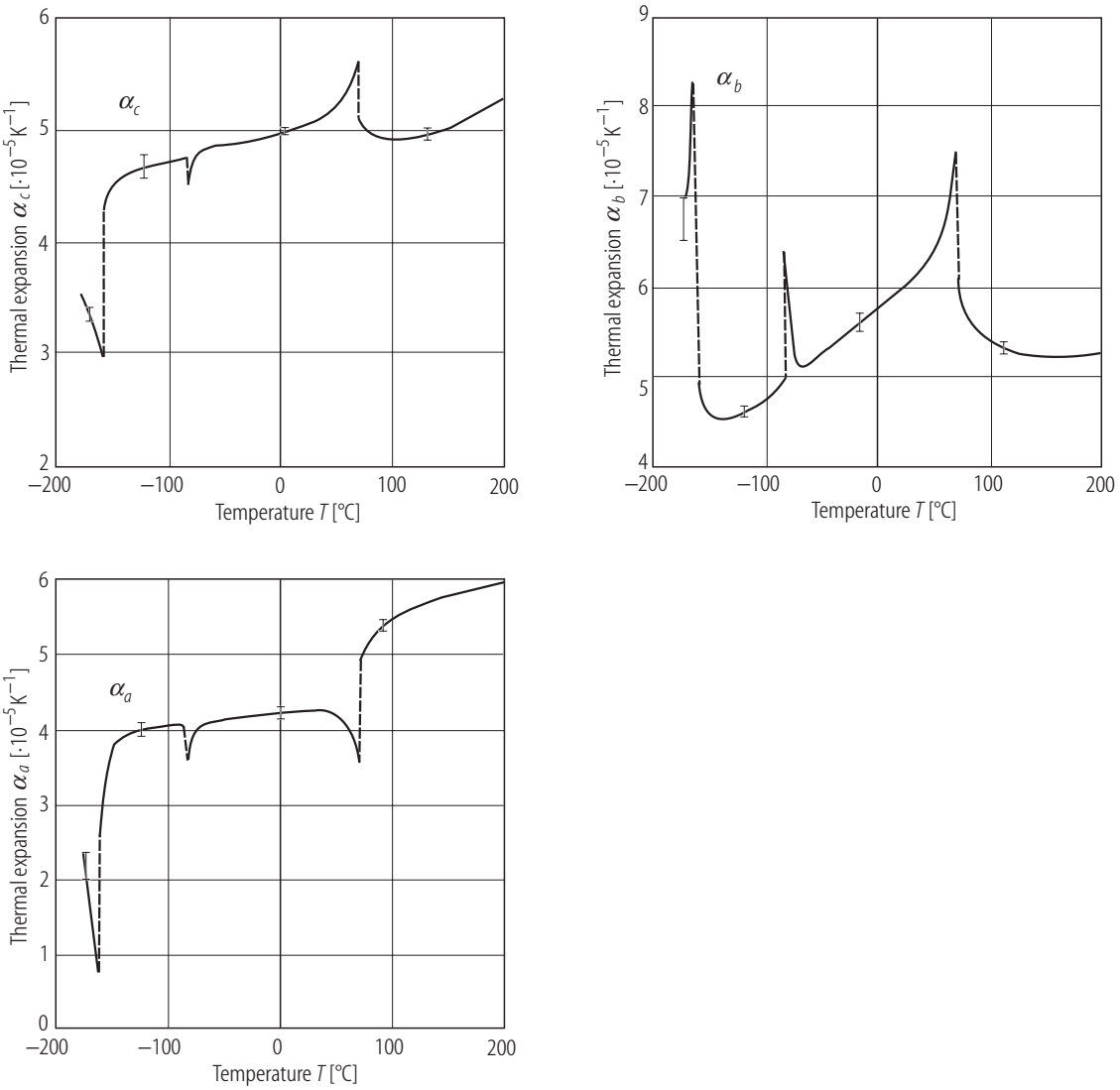

Fig. 39A-17-003. Rb_2ZnBr_4. α_a, α_b, α_c vs. T [90Iva]. α_a, α_b, α_c: linear thermal expansion coefficients along the *a*, *b* and *c* axes.

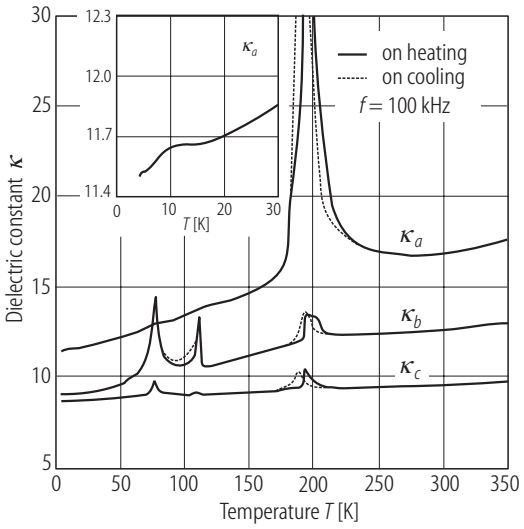

Fig. 39A-17-004. Rb_2ZnBr_4. κ_a, κ_b, κ_c vs. T [91Yam]. f = 100 kHz. Insert: κ_a vs. T below 35 K.

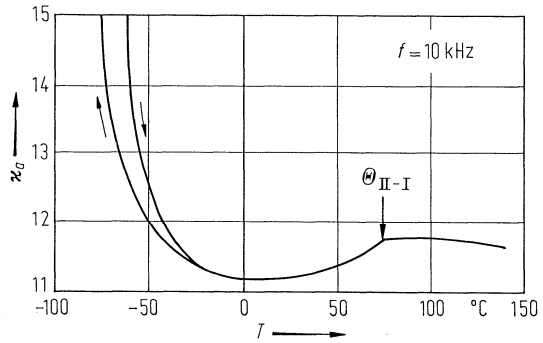

Fig. 39A-17-005. Rb_2ZnBr_4. κ_a vs. T [81Ham]. f = 10 kHz.

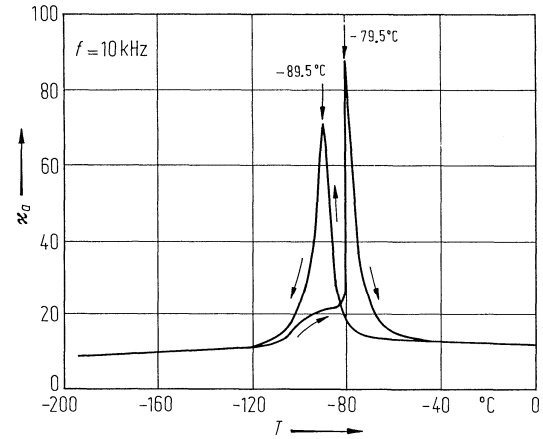

Fig. 39A-17-006. Rb_2ZnBr_4. κ_a vs. T [81Ham]. f = 10 kHz.

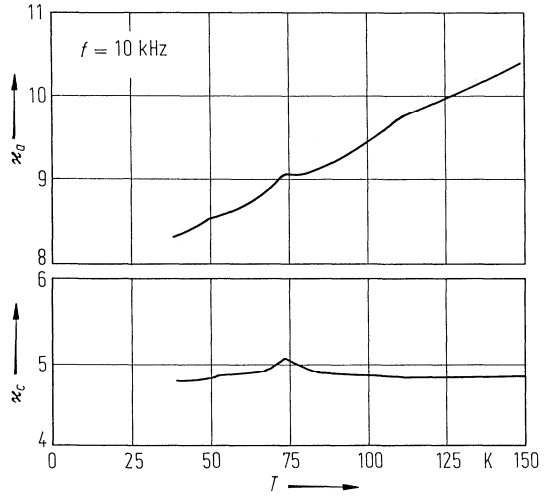

Fig. 39A-17-007. Rb_2ZnBr_4. $\varkappa_a$, $\varkappa_c$ vs. T [82Yam]. f = 10 kHz.

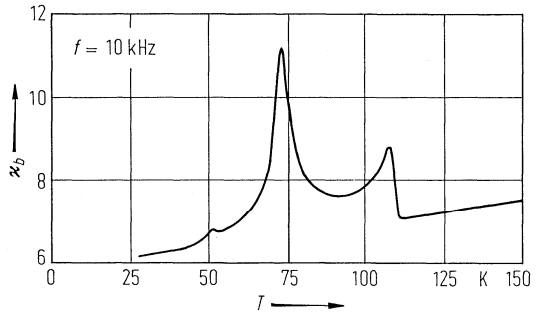

Fig. 39A-17-008. Rb_2ZnBr_4. $\varkappa_b$ vs. T [82Yam]. f = 10 kHz.

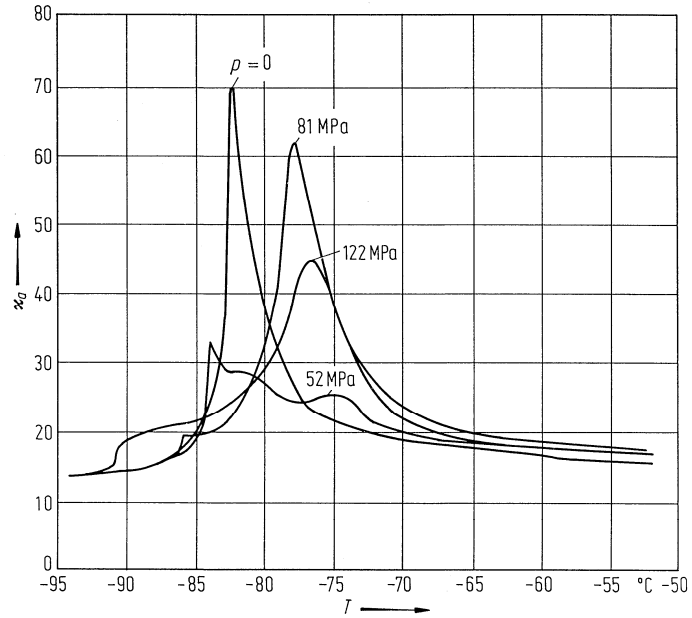

Fig. 39A-17-009. Rb_2ZnBr_4. $\varkappa_a$ vs. T on cooling [85Ges]. Parameter: p.

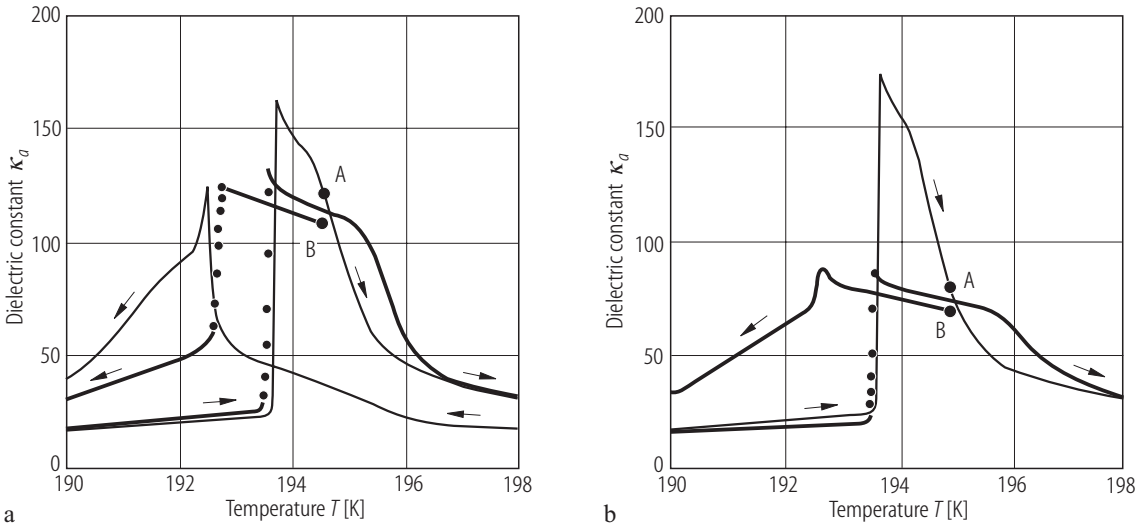

Fig. 39A-17-010. Rb_2ZnBr_4. Memory effect in κ_a vs. T [88Fol]. On a heating run, temperature was stopped at a given point A and held for 20 hours. After the annealing (point B), κ_a was measured on cooling and heating run. Thin lines represent the normal behavior observed at constant rate of 0.1 K/min. The results for two holding temperatures are shown in (**a**) and (**b**).

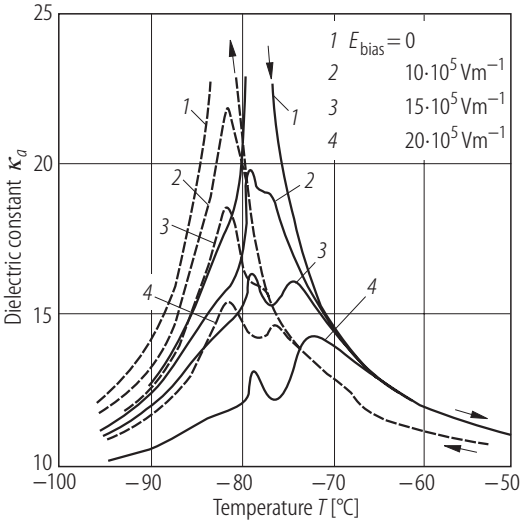

Fig. 39A-17-011. Rb_2ZnBr_4. κ_a vs. T [88Kro]. Parameter: E_{bias}. f = 1592 Hz. Cooling and heating rate was 0.5 K/min. The maximum value of κ_a was about 40 for E_{bias} = 0.

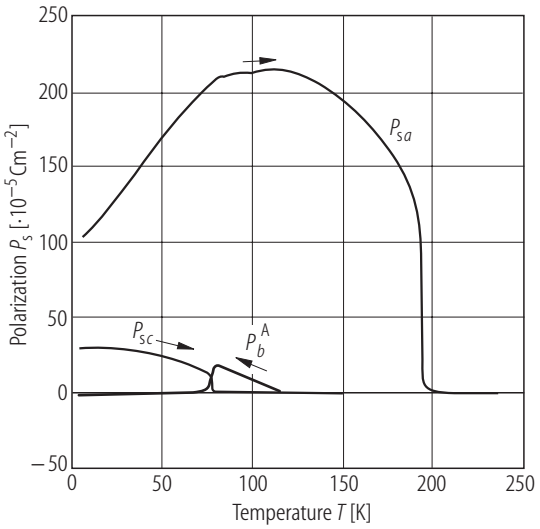

Fig. 39A-17-012. Rb_2ZnBr_4. P_{sa}, P_b^A, P_{sc} vs. T [91Yam]. Pyroelectric charge measurements on heating. P_{sa}, P_{sc}: spontaneous polarization along the *a* and *c* axes, respectively. P_b^A : polarization along the *b* axis, see also Fig. 39A-17-013.

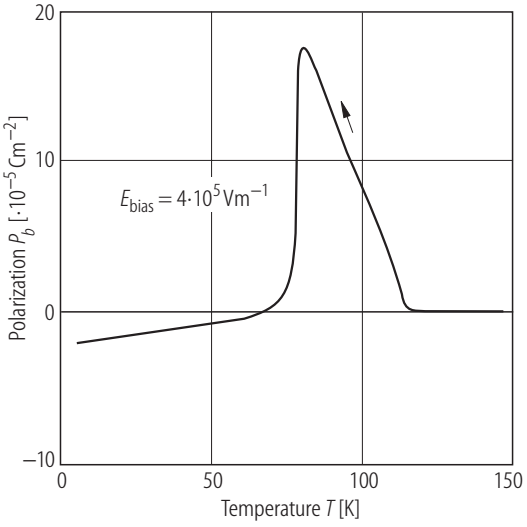

Fig. 39A-17-013. Rb_2ZnBr_4. P_b vs. T [91Yam]. P_b: polarization induced by electric field along the *b* axis, $E_{bias} = 4 \cdot 10^5$ V m^{-1}. Pyroelectric charge measurements on cooling.

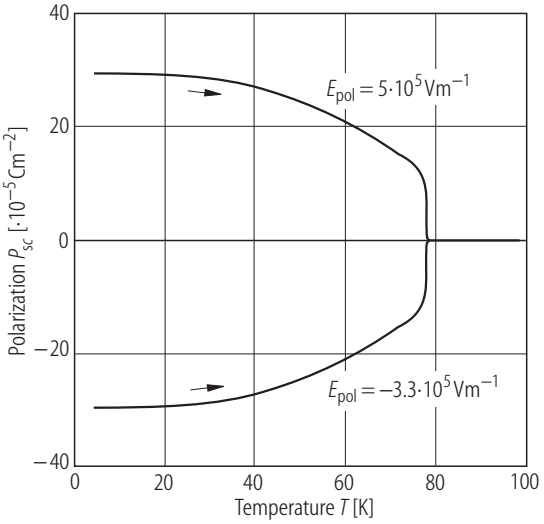

Fig. 39A-17-014. Rb_2ZnBr_4. P_{sc} vs. T [91Yam]. P_{sc}: spontaneous polarization along the c axis, E_{pol}: poling field. Pyroelectric charge measurements.

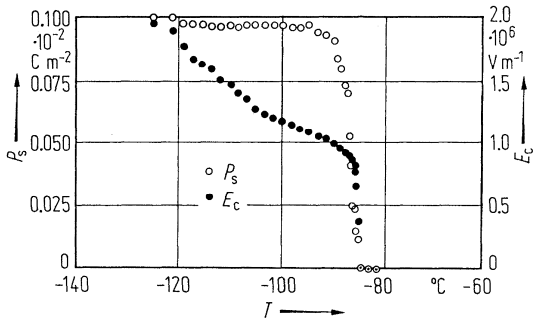

Fig. 39A-17-015. Rb_2ZnBr_4. P_s, E_c vs. T [77Saw]. P_s: spontaneous polarization along the a axis.

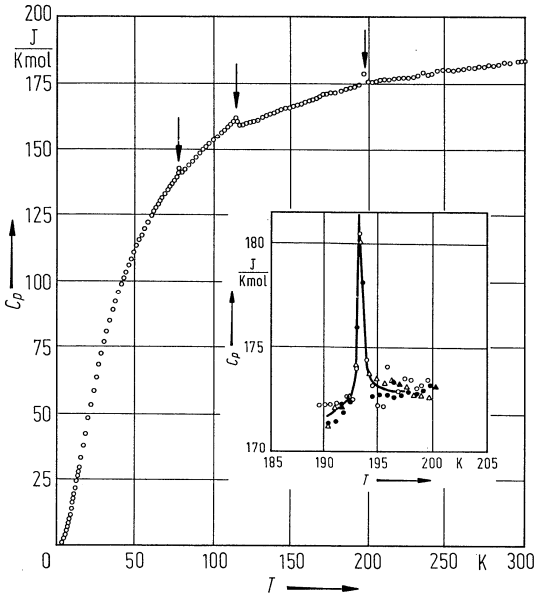

Fig. 39A-17-016. Rb_2ZnBr_4. C_p vs. T [83Nom]. C_p: molar heat capacity at constant pressure. In the insert, each series of measurements is represented by a different mark.

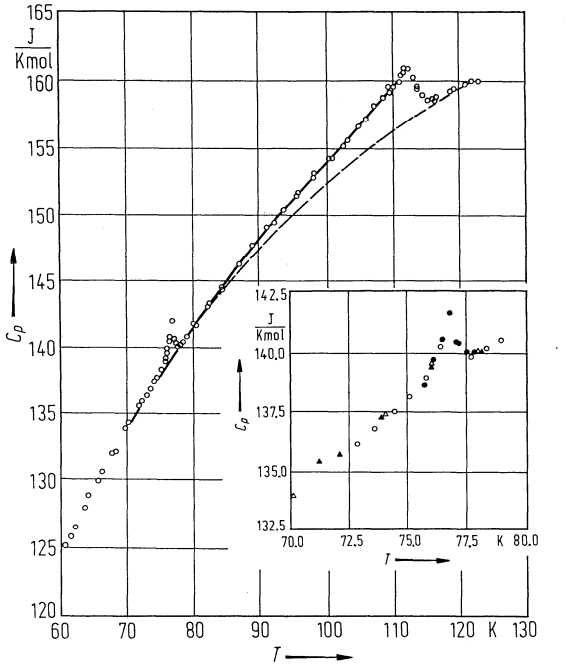

Fig. 39A-17-017. Rb_2ZnBr_4. C_p vs. T near the lower transitions [83Nom]. C_p: molar heat capacity at constant pressure. In the insert, each series of measurements is represented by a different mark.

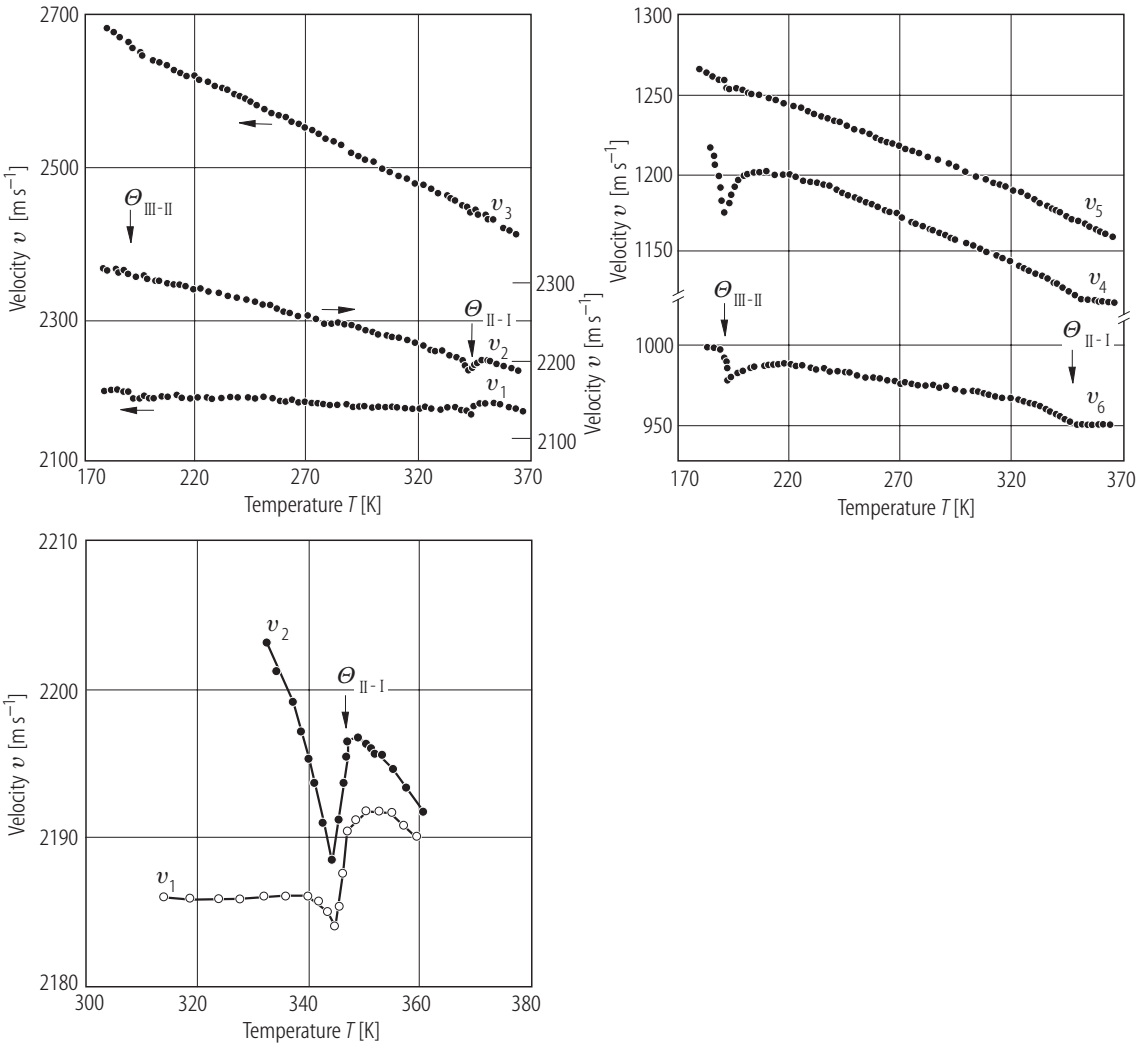

Fig. 39A-17-018. Rb_2ZnBr_4. v vs. T [93Kit2]. v_λ: sound velocity corresponding to $c_{\lambda\lambda}$ mode. f = 10 MHz.

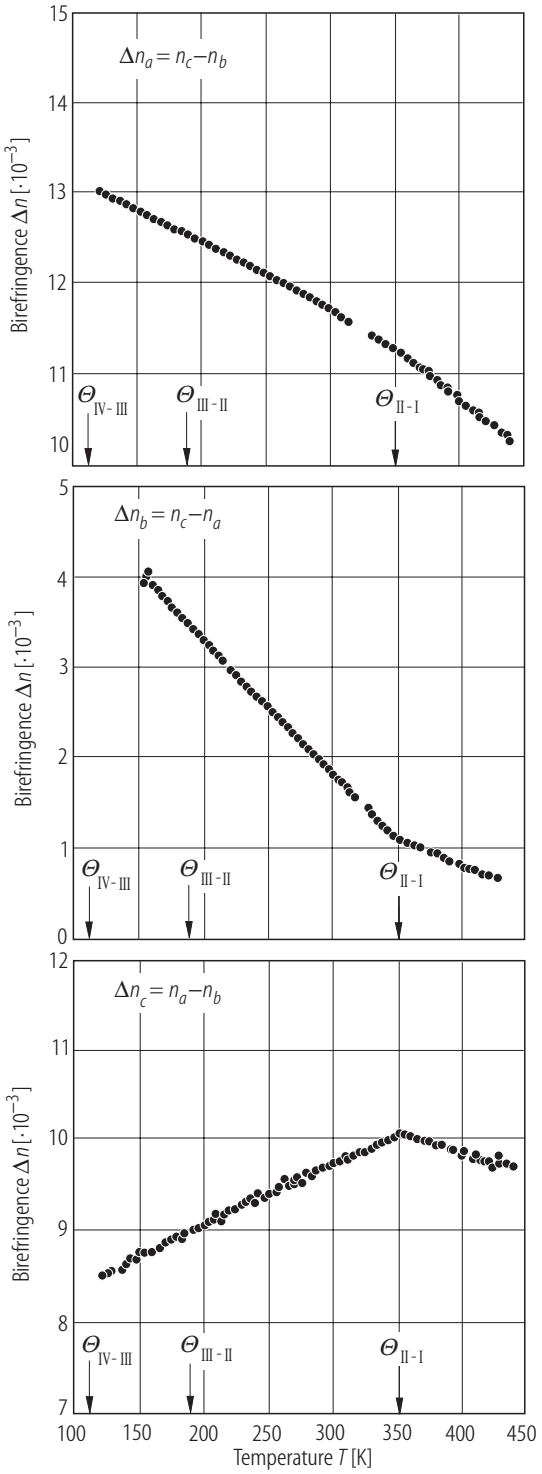

Fig. 39A-17-019. Rb_2ZnBr_4. Δn vs. T [94Kob]. $\lambda = 6328$ Å.

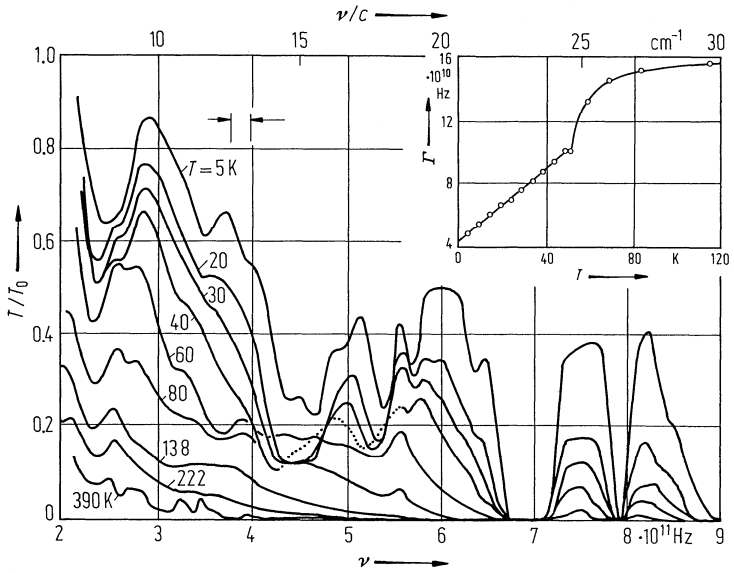

Fig. 39A-17-020. Rb_2ZnBr_4. T/T_0 vs. ν [82Ras]. Parameter: T. T/T_0: transmission of far-infrared radiation along the c axis. Resolution of the spectra is shown by the arrows. The insert is Γ vs. T. Γ: damping of the 23 cm^{-1} mode.

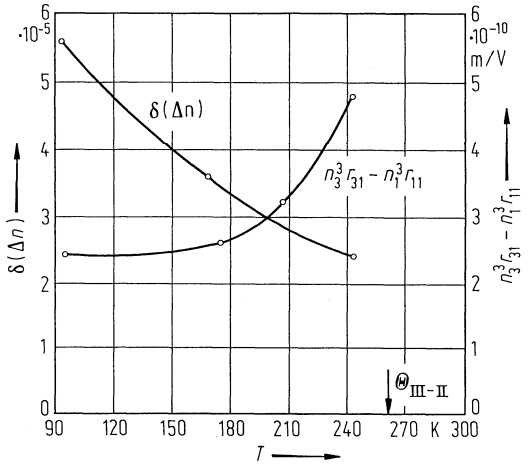

Fig. 39A-17-021. Rb_2ZnBr_4. $\delta(\Delta n)$, $n_3^3 r_{31} - n_1^3 r_{11}$ vs. T [80Nak]. $\delta(\Delta n)$: change in birefringence $\Delta n = n_3 - n_1$ upon illuminating with 313 nm wavelength light. $\lambda = 632.8$ nm. $r_{\lambda i}$: electrooptic constant.

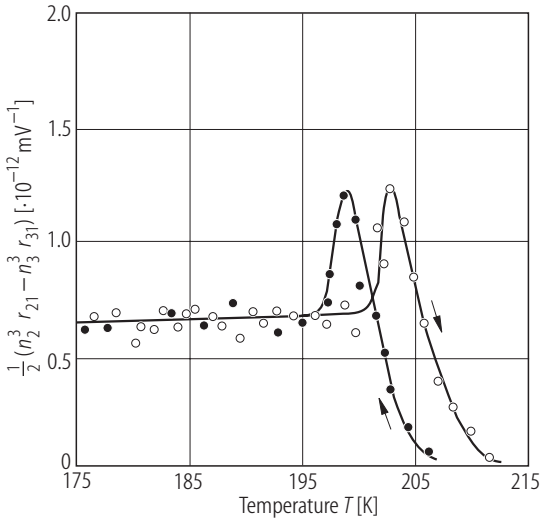

Fig. 39A-17-022. Rb_2ZnBr_4. $(n_2^3 r_{21} - n_3^3 r_{31})/2$ vs. T [89Vlo]. $\lambda = 633$ nm. $r_{\lambda i}$: electrooptic constant.

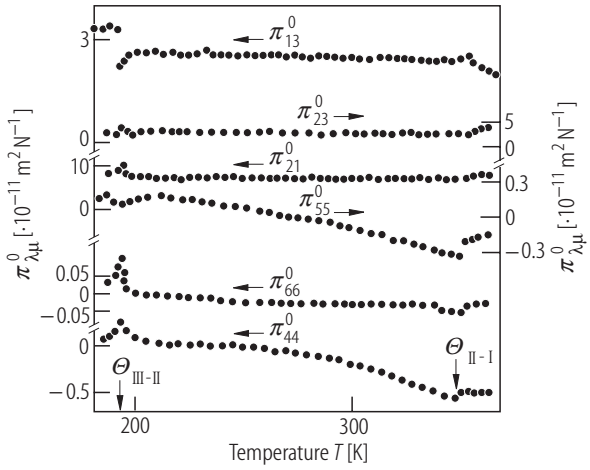

Fig. 39A-17-023. Rb_2ZnBr_4. $\pi^0_{\lambda\mu}$ vs. T [89Vlo]. $\pi^0_{\lambda\mu}$: effective piezooptic constant;
$\pi^0_{13} = n_2^3\pi_{23} - n_3^3\pi_{33}$, $\pi^0_{21} = n_3^3\pi_{31} - n_1^3\pi_{11}$, $\pi^0_{23} = n_3^3\pi_{33} - n_1^3\pi_{13}$, $\pi^0_{44} = \sqrt{2}n_2^3 n_3^3\pi_{44}/(n_2^2 + n_3^2)^{3/2}$,
$\pi^0_{55} = \sqrt{2}n_1^3 n_3^3\pi_{55}/(n_1^2 + n_3^2)^{3/2}$, $\pi^0_{66} = \sqrt{2}n_1^3 n_2^3\pi_{66}/(n_1^2 + n_2^2)^{3/2}$. $\lambda = 633$ nm. $\pi_{\lambda\mu}$: piezooptic constant.

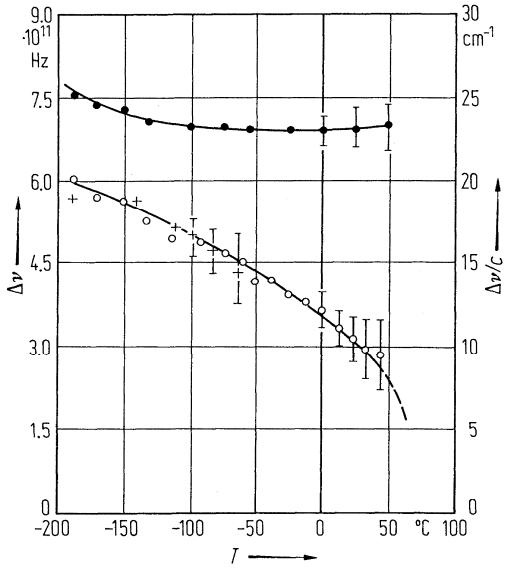

Fig. 39A-17-024. Rb_2ZnBr_4. $\Delta\nu$ vs. T [80Tak]. $\Delta\nu$: Raman shift. Open and full circles: $b(aa)c$ geometry. Crosses: $a(cc)b$ geometry.

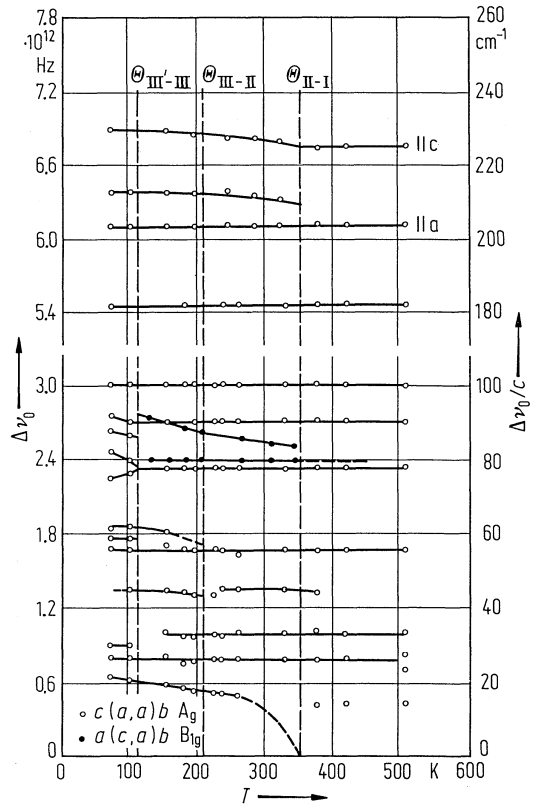

Fig. 39A-17-025. Rb_2ZnBr_4. $\Delta\nu_0$ vs. T [82Ras]. $\Delta\nu_0$: Raman shift of A_g modes observed in the scattering geometry $c(aa)b$ and B_{1g} modes observed in the $a(ca)b$ geometry.

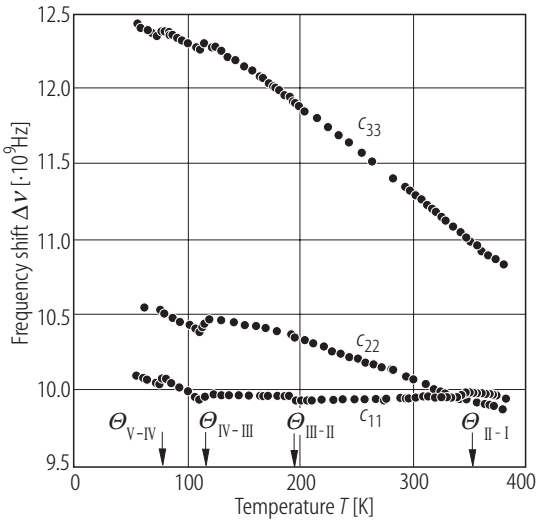

Fig. 39A-17-026. Rb_2ZnBr_4. $\Delta\nu$ vs. T [89Hor]. $\Delta\nu$: Brillouin shift of LA mode.

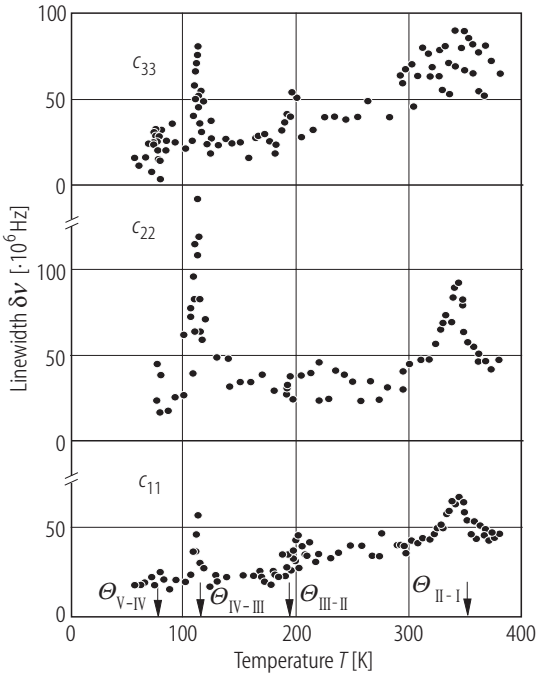

Fig. 39A-17-027. Rb_2ZnBr_4. $\delta\nu$ vs. T [89Hor]. $\delta\nu$: half width at half maximum of Brillouin spectrum of LA mode.

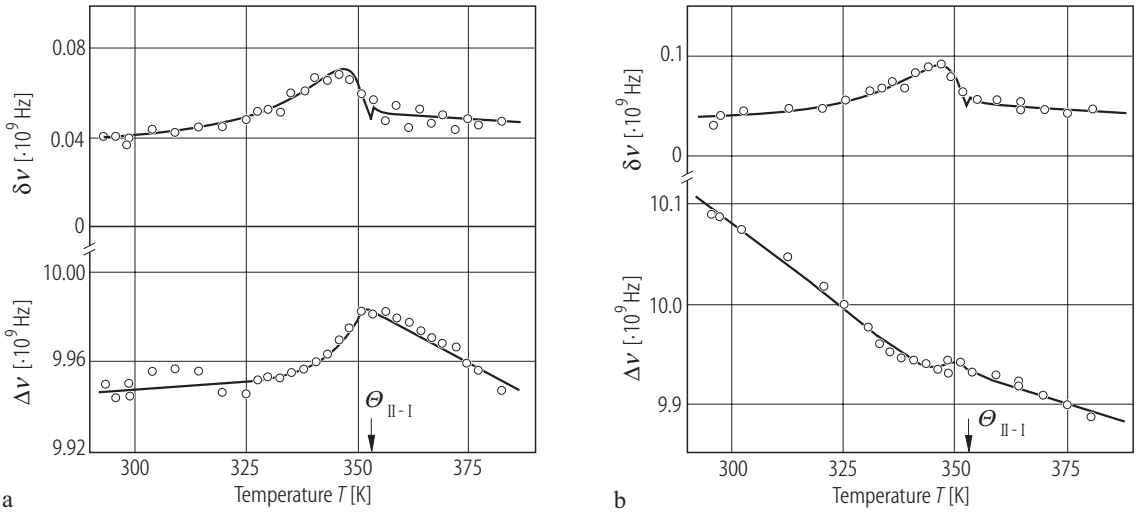

Fig. 39A-17-028. Rb_2ZnBr_4. $\Delta\nu$, $\delta\nu$ vs. T [89Hor]. $\Delta\nu$: Brillouin shift. $\delta\nu$: half width at half maximum of Brillouin spectrum. (**a**) c_{11}-mode; (**b**) c_{22}-mode.

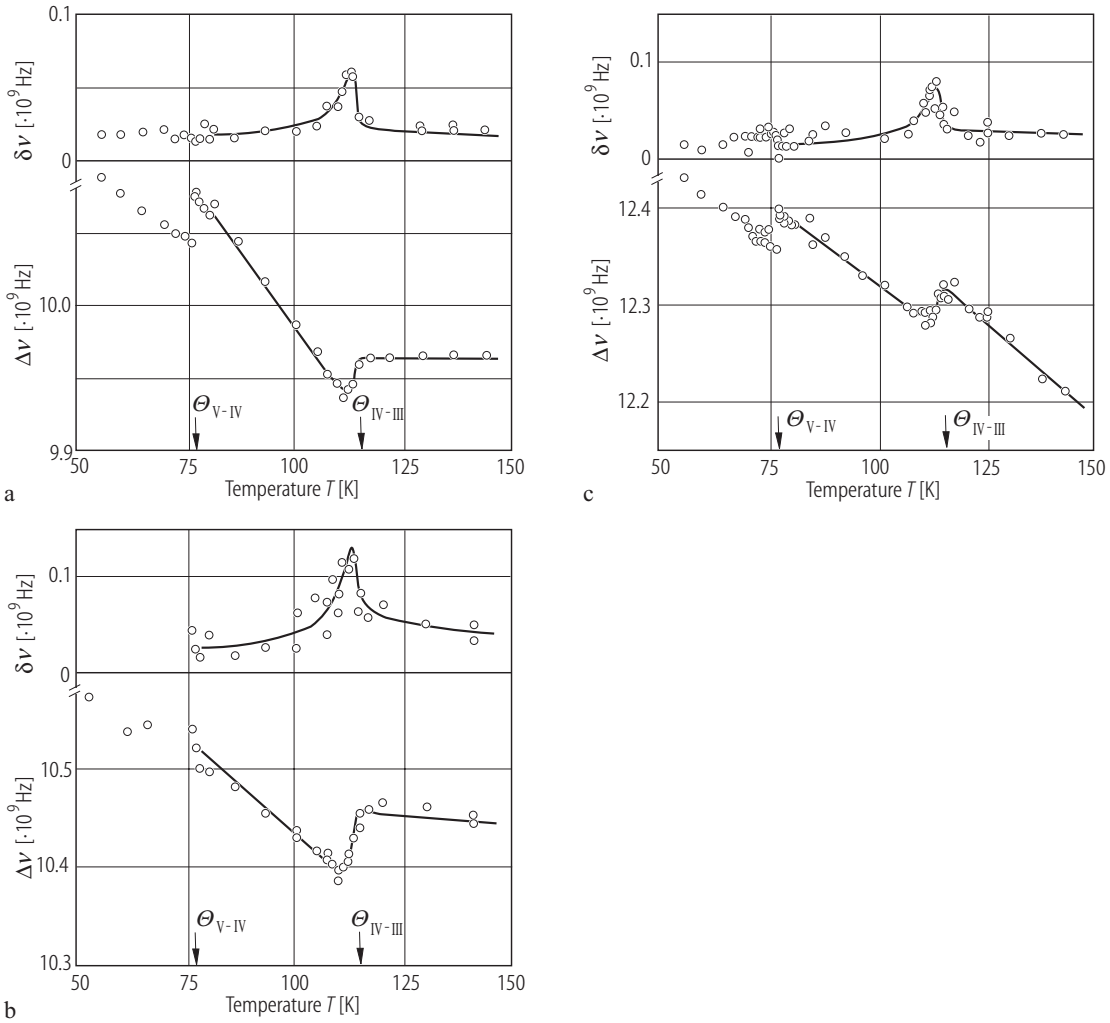

Fig. 39A-17-029. Rb_2ZnBr_4. $\Delta\nu$, $\delta\nu$ of LA mode vs. T [89Hor]. $\Delta\nu$: Brillouin shift. $\delta\nu$: half width at half maximum of Brillouin spectrum. (**a**) c_{11}-mode; (**b**) c_{22}-mode; (**c**) c_{33}-mode.

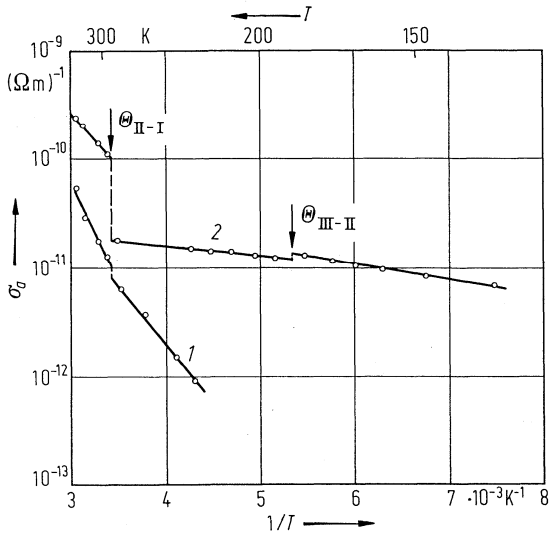

Fig. 39A-17-030. Rb_2ZnBr_4. σ_a vs. T^{-1} [80Nak]. σ_a: conductivity along the *a* axis. Curve *1* is dark conductivity, curve *2* is photoconductivity measured under the illumination of 313 nm wavelength light.

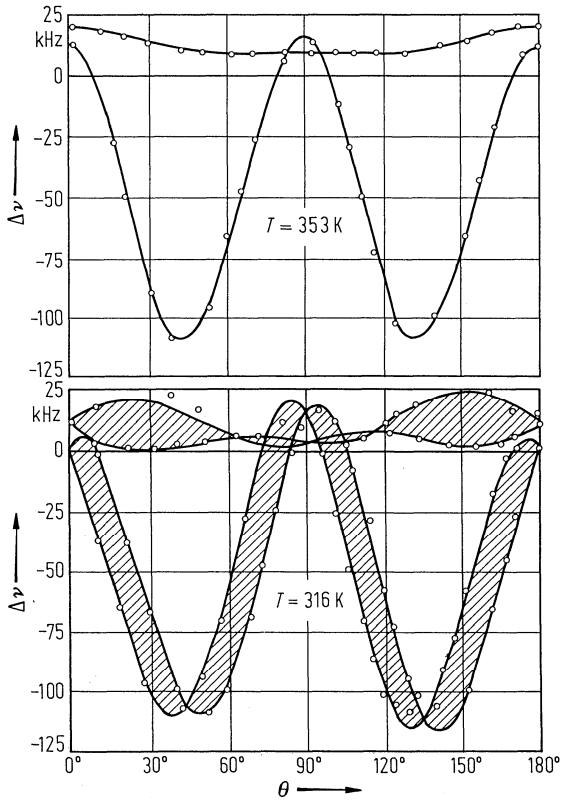

Fig. 39A-17-031. Rb_2ZnBr_4. $\Delta\nu$ vs. θ [82Rut]. $\Delta\nu$: second-order quadrupolar shifts of ^{87}Rb 1/2 → –1/2 spectra. θ: angle between $\boldsymbol{H}$ and the *a* axis in (010). $\boldsymbol{H} \perp \boldsymbol{b}$. ν_L = 29.5 MHz. Hatched regions indicate continuous broad spectra.

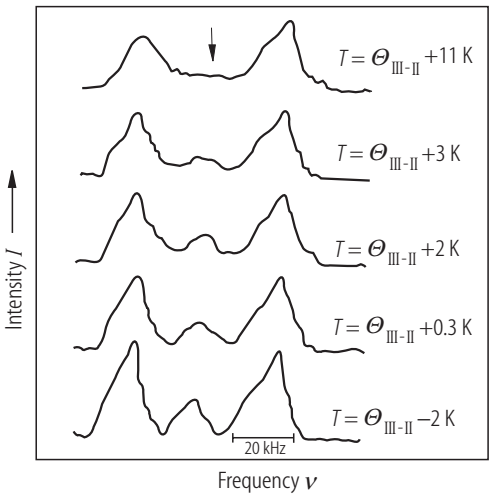

Fig. 39A-17-032. Rb_2ZnBr_4. ^{87}Rb 1/2 → −1/2 spectra in the vicinity of Θ_{III-II} [82Rut]. ν_L = 29.5 MHz. Thick arrow indicates the appearance of a commensurate line. $\boldsymbol{H} \perp \boldsymbol{b}$. $\angle(\boldsymbol{H}, \boldsymbol{a}) = 162°$.

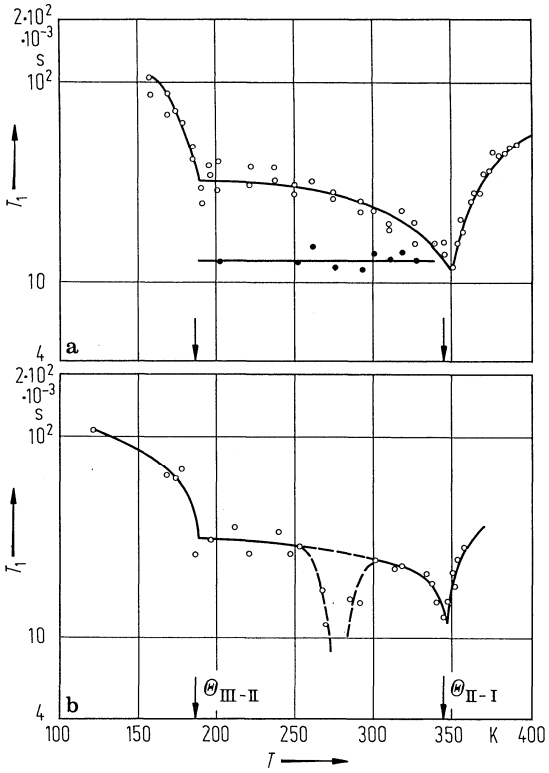

Fig. 39A-17-033. Rb_2ZnBr_4. T_1 vs. T [82Rut]. T_1: spin-lattice relaxation time of ^{87}Rb. Open circles: obtained at edge singularity. Full circles: obtained in the middle of the frequency distribution. ν_L = 88.3 MHz. (**a**) $\boldsymbol{H} \perp \boldsymbol{b}$, $\angle(\boldsymbol{H}, \boldsymbol{c}) = 60°$; (**b**) $\boldsymbol{H} \perp \boldsymbol{a}$, $\angle(\boldsymbol{H}, \boldsymbol{c}) = 65°$.

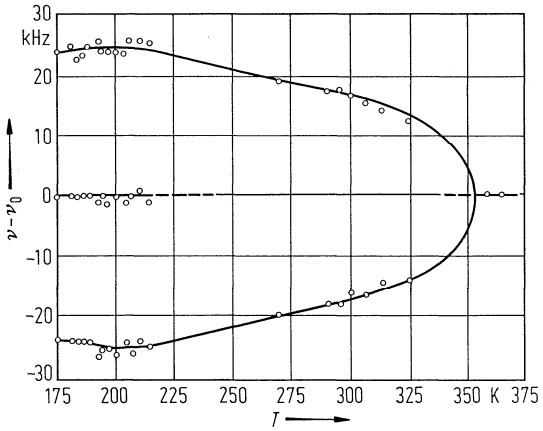

Fig. 39A-17-034. Rb_2ZnBr_4. $\nu-\nu_0$ vs. T [86Bli1]. ν: NMR resonance frequency of ^{87}Rb 1/2 → −1/2 spectra. ν_0: resonance frequency in phase I. $\boldsymbol{H} \perp \boldsymbol{b}$. $\angle(\boldsymbol{H}, \boldsymbol{a}) = 162°$. $\nu_L = 29.5$ MHz.

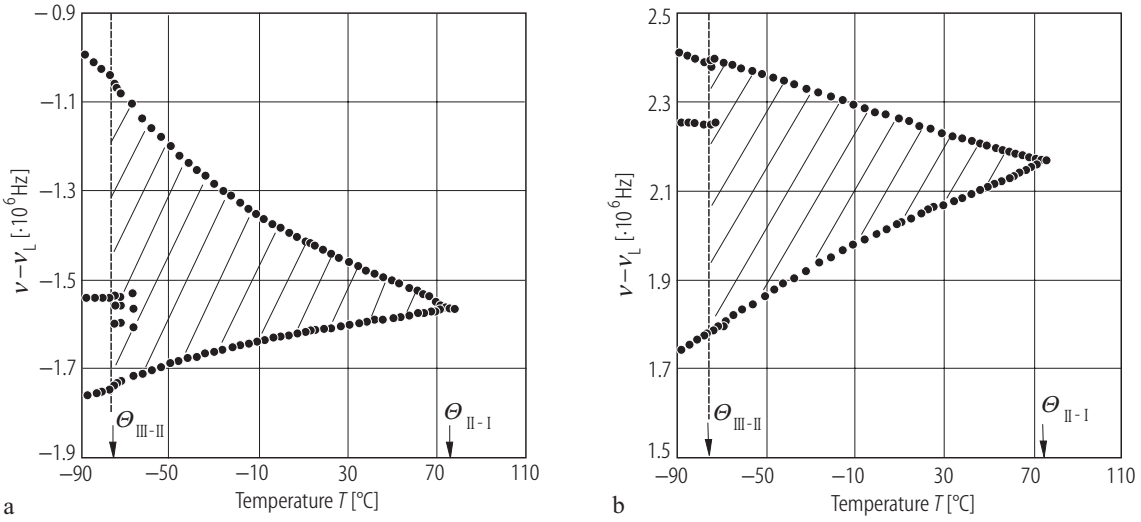

Fig. 39A-17-035. Rb_2ZnBr_4. $\nu-\nu_L$ vs. T [87Wal]. ν: NMR resonance frequency of one satellite transition of ^{87}Rb. (**a**) Rb(2), $\boldsymbol{H} \parallel \boldsymbol{b}$, on cooling; (**b**) Rb(1), $\boldsymbol{H} \parallel \boldsymbol{a}$, on heating. ν_L = 98.2 MHz. The hatched areas represent the background spectra in phase II.

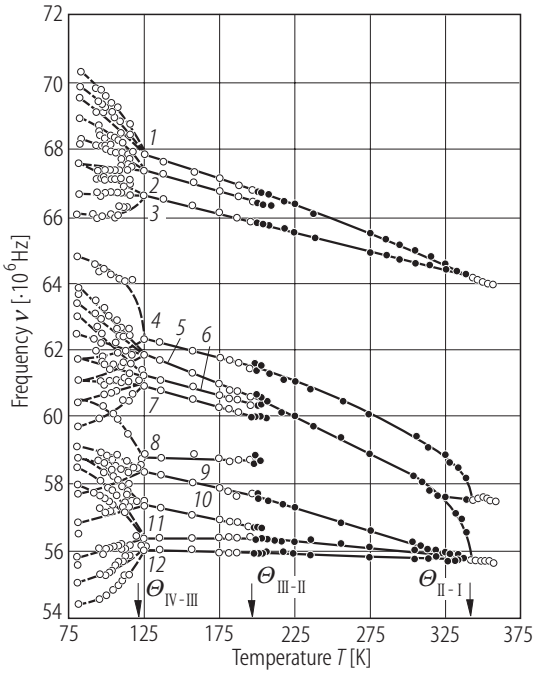

Fig. 39A-17-036. Rb_2ZnBr_4. ν vs. T [81Bel]. ν: ^{81}Br NQR frequency. Numerals 1 to 12 shown in the ferroelectric phase III ($\Theta_{IV-III} < T < \Theta_{III-II}$) indicate the twelve independent signals, which split into 32 signals in phase IV. Full circles denote those in the incommensurate phase ($\Theta_{III-II} < T < \Theta_{II-I}$).

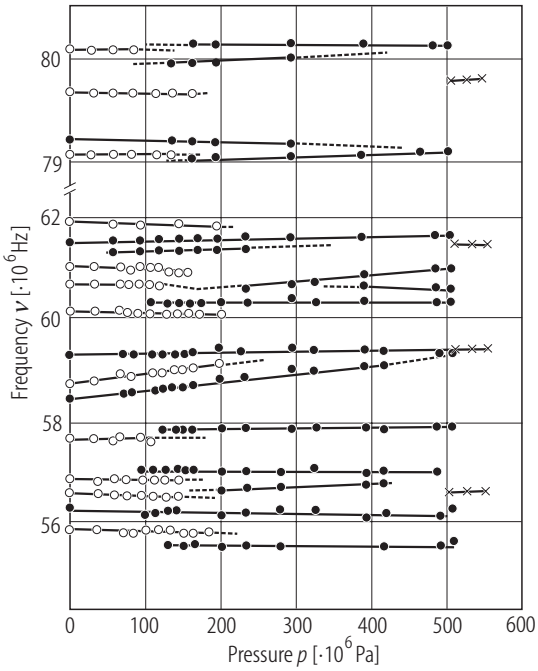

Fig. 39A-17-037. Rb_2ZnBr_4. ν vs. p at 173 K [88Ale]. ν: ^{81}Br NQR frequency. Open circle, full circle and cross are the data of phase III, intermediate and high-pressure phases, respectively.

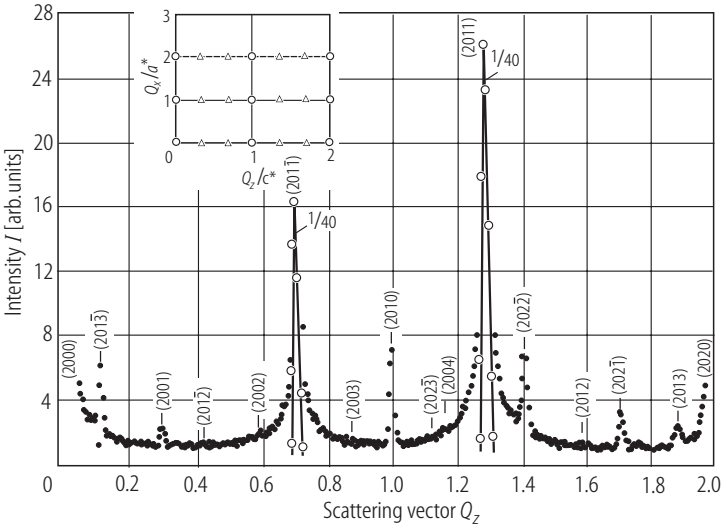

Fig. 39A-17-038. Rb_2ZnBr_4. I vs. Q_z at 25 °C [83Iiz]. I: intensity of neutron scattering. Q_z: z component of the scattering vector in unit of c^*. The scanning line is illustrated in the insert by the broken line. Misfit parameter $\delta = 0.040$.

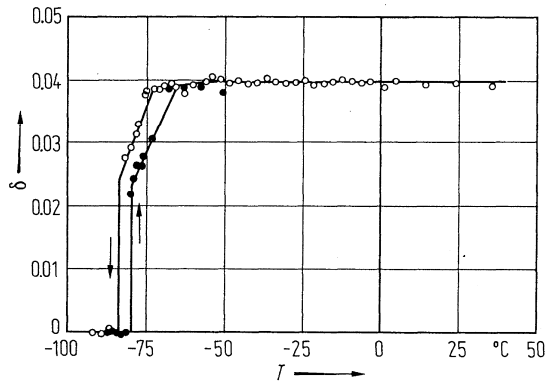

Fig. 39A-17-039. Rb_2ZnBr_4. δ vs. T [78Ges]. δ: misfit parameter.

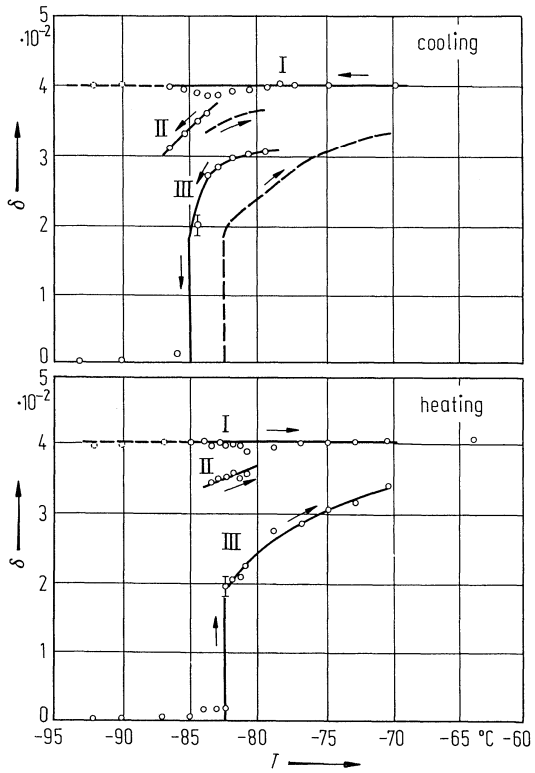

Fig. 39A-17-040. Rb_2ZnBr_4. δ vs. T [83Iiz]. δ: misfit parameter for peaks I, II and III constituting $20\,1\,\overline{3}$ satellite of neutron scattering. Upper half: on cooling, lower half: on heating. The heating results are also indicated by the dashed lines in the upper half for comparison. The dotted circles indicate the trace of the persisting peak at low temperature.

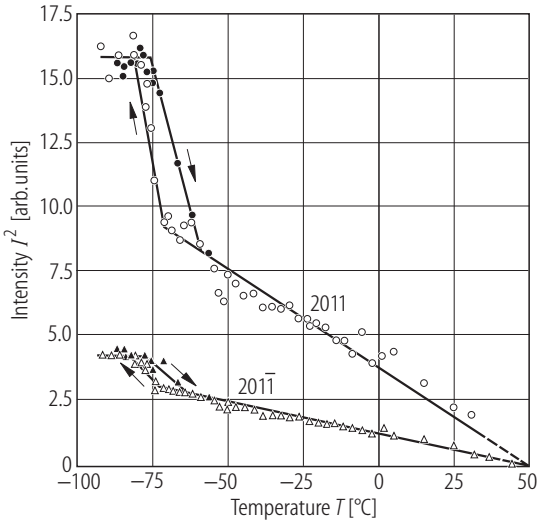

Fig. 39A-17-041. Rb_2ZnBr_4. I^2_{2011}, $I^2_{20\bar{1}\bar{1}}$ vs. T [78Ges]. I_{2011}, $I_{20\bar{1}\bar{1}}$: integrated intensity of 2011 and $20\,\bar{1}\,\bar{1}$ satellite of neutron scattering. Note Θ_{II-I} is 50 °C in this experiment.

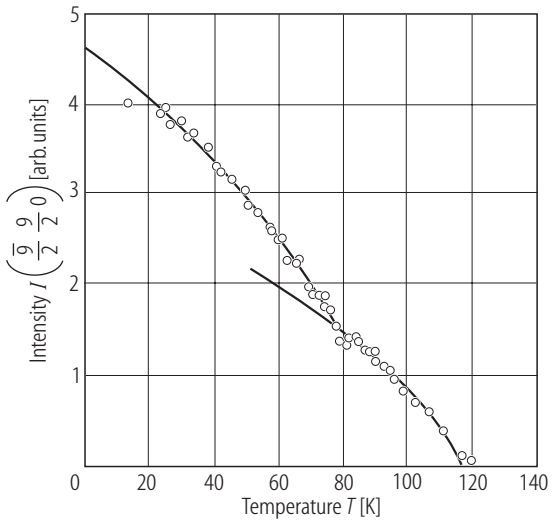

Fig. 39A-17-042. Rb_2ZnBr_4. $I(\bar{9}/2, 9/2, 0)$ vs. T [94Kas]. $I(\bar{9}/2, 9/2, 0)$: integrated intensity of $\bar{9}/2, 9/2, 0$ satellite of neutron diffraction on a heating run. The reflection is indexed referring to the lattice of phase I.

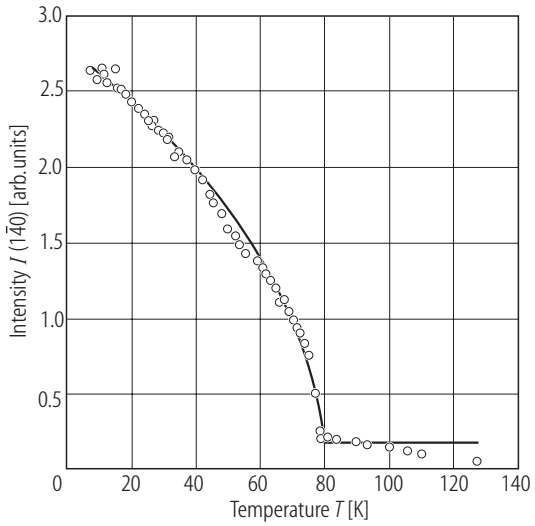

Fig. 39A-17-043. Rb_2ZnBr_4. $I(1\bar{4}0)$ vs. T [96Shi2]. $I(1\bar{4}0)$: integrated intensity of $1\bar{4}0$ reflection on a heating run. Neutron diffraction. The reflection is indexed referring to the lattice of phase I.

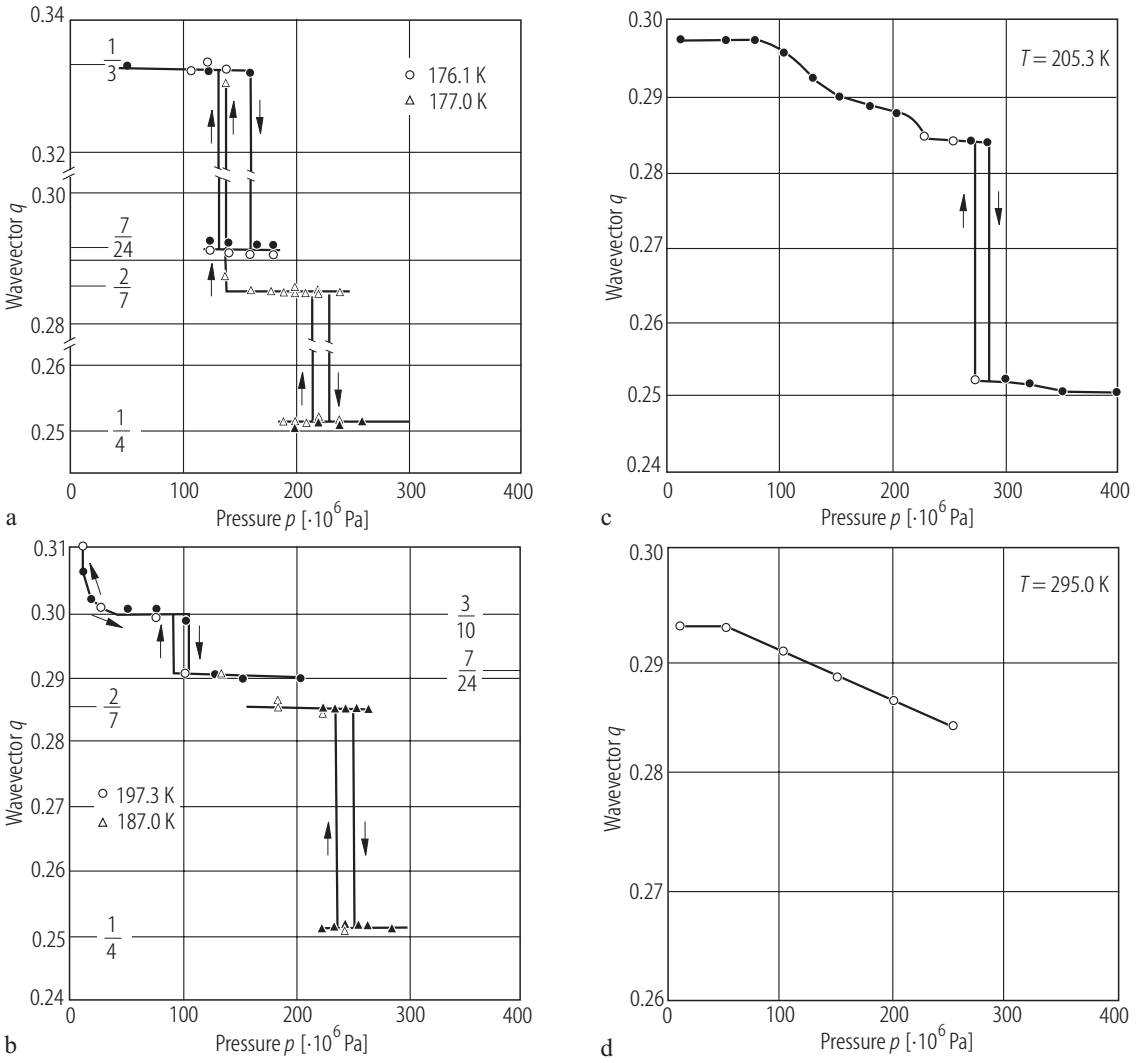

Fig. 39A-17-044. Rb_2ZnBr_4. q vs. p [92Par]. q: modulation wave vector in unit of c^*. (**a**) 176.1 and 177.0 K; (**b**) 187.0 and 197.3 K; (**c**) 205.3 K; (**d**) 295.0 K. Solid and open symbols correspond to increasing and decreasing pressure runs, respectively.

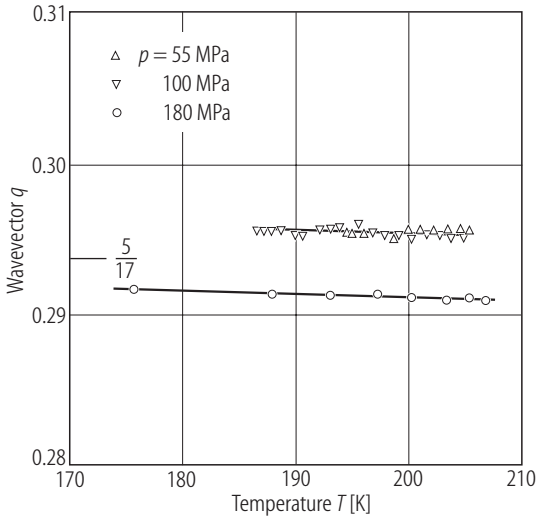

Fig. 39A-17-045. Rb_2ZnBr_4. q vs. T [92Par]. q: modulation wave vector in unit of c^*. Parameter: p; p = 55 MPa (cooling), p = 100 MPa (heating), p = 180 MPa (heating and cooling), respectively.

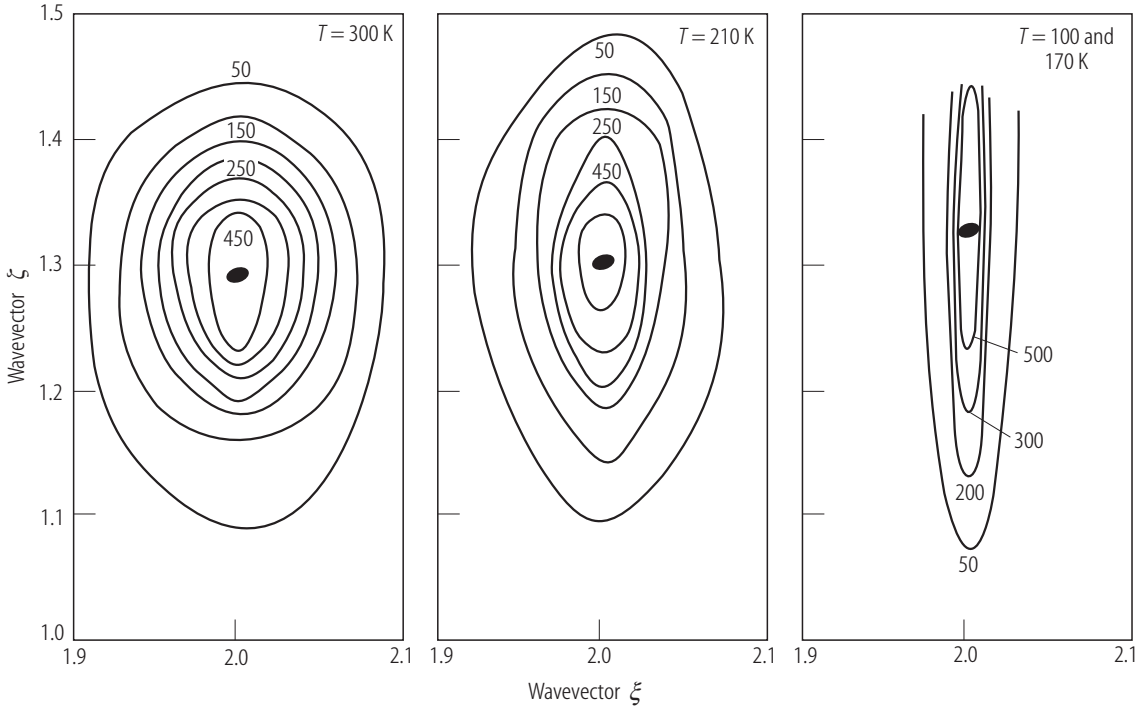

Fig. 39A-17-046. Rb_2ZnBr_4. Intensity contours of neutron diffuse scattering on (ξ, 0, ζ) plane [in arbitrary units] [79deP2]. Parameter: T. The background intensity has been subtracted. The ellipse at the satellite position represents the resolution function. The peak intensity of the satellite is about $3 \cdot 10^5$.

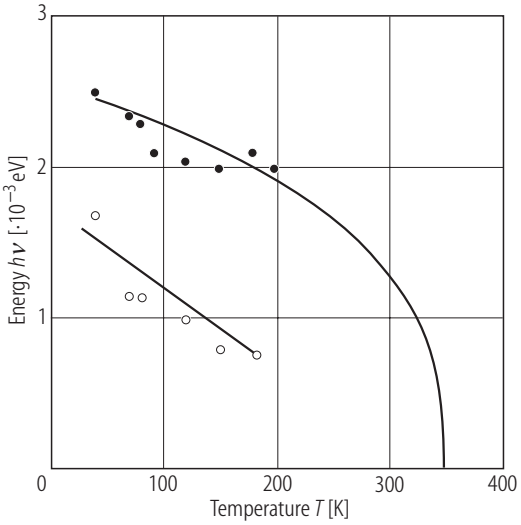

Fig. 39A-17-047. Rb_2ZnBr_4. $h\nu$ vs. T [96Mas]. ν: phonon frequency of phase mode (open circle) and amplitude mode (full circle).

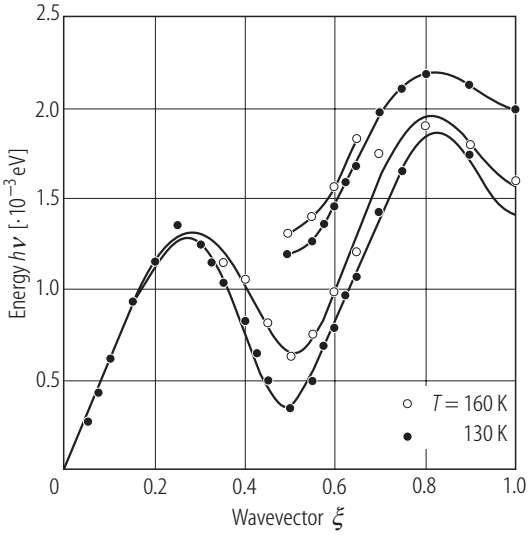

Fig. 39A-17-048. Rb_2ZnBr_4. Phonon dispersion in an extended zone scheme along the [ξ, ξ, 0] direction at 130 K and 160 K [96Shi2].

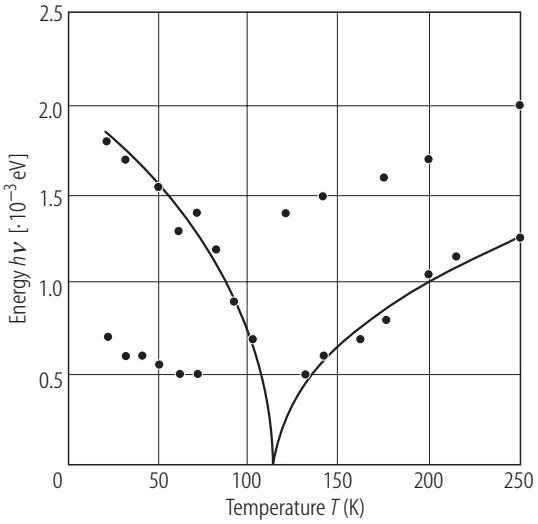

Fig. 39A-17-049. Rb_2ZnBr_4. $h\nu$ vs. T [95Mas]. ν: phonon frequency at $\boldsymbol{k} = (\boldsymbol{a}^* + \boldsymbol{b}^*)/2$.